PHILOSOPHICAL TRANSACTIONS OF THE ROYAL SOCIETY A MATHEMATICAL, PHYSICAL & ENGINEERING SCIENCES

Some Topical Issues in Research on Short-Pulse Laser-Produced Plasmas [and Discussion]

M. H. Key and C. Yamanaka

Phil. Trans. R. Soc. Lond. A 1980 **298**, 351-364
doi: 10.1098/rsta.1980.0259

Phil. Trans. R. Soc. Lond. A **298**, 351–364 (1980)
Printed in Great Britain

Some topical issues in research on short-pulse laser-produced plasmas

By M. H. Key†
Queen's University, Belfast, U.K.

[Plate 1]

A brief review is presented of the main physical processes in laser-produced plasmas. This is followed by illustrations taken from recent work at the S.R.C. Central Laser Facility of the use of X-ray and visible streak cameras for fast time resolved measurements of implosion and interaction phenomena in laser-produced plasmas.

1. Introduction

Since the main influence on the development of short-pulse high-power lasers has been the need for increased intensity and power for laser-produced plasma and laser fusion research, and as a prelude to papers in this meeting discussing high power lasers, § 2 of this paper gives a background review for the non-specialist of the main physical processes in laser-produced plasmas.

Section 3 of the paper is concerned with ultra-short time scale measurements in the study of laser-produced plasmas, with emphasis on new streak camera techniques. The development of X-ray sensitive streak cameras was motivated by the need to time-resolve X-ray emission from laser-driven implosions, and recent work in this field is described. Streak cameras with conventional photocathodes have also been of value in recording fundamental and harmonic frequency laser light generated in high-intensity laser–plasma interactions. Illustrations of progress in these areas of research are presented by using results from the Science Research Council Central laser facility (C.L.F.). The C.L.F. has a powerful (0.6 TW) two-beam Nd : glass laser and is a centre for research by U.K. universities. It could be said that the same strong interest in the U.K. in ultra-short pulses that has inspired the present Royal Society Meeting also led to the rapid progress in streak camera studies of laser-produced plasma at the C.L.F. which are described here.

2. Physical processes in laser-produced plasmas

Focused beam intensities in the range 10^{13} to 10^{17} W cm^{-2} are achieved with modern high power lasers. Nd : glass, CO_2 and iodine lasers can produce single beam powers of over 1 TW at wavelength, λ, of 1.06, 10.6 and 1.3 μm respectively. These high-power beams can be focused to spot diameters of the order of 10–20 λ, limited by the imperfections of large diameter optics and of the wavefront of the laser beam.

The detailed features of laser-produced plasmas vary with laser intensity, focal spot size, pulse duration, target geometry and material and laser wavelength. A qualitative description of their main physical processes can be developed with reference to figure 1, which shows

† Present address: Laser Division, S.R.C. Rutherford Laboratory, Chilton, Didcot, Oxon. OX11 0QX, U.K.

schematically the distributions of plasma density ρ and of electron temperature T_e prevailing in a typical plasma. The magnitudes of relevant parameters which would produce a nearly steady plasma flow distribution such as that shown in figure 1 are of order 10^{15} W cm^{-2} of $\lambda = 1$ μm irradiation of duration more than 100 ps on a low atomic number Z solid sphere of 100 μm diameter.

(*a*) *Critical density*

Laser radiation entering the plasma flowing from the irradiated surface in figure 1 encounters increasing density of plasma. Where the resonant frequency of the plasma electrons in an oscillatory electric field is equal to the laser frequency, the plasma refractive index becomes zero, electromagnetic (e.m.) wave propagation ceases and reflexion occurs. Plasma electrons cause essentially all the dielectric behaviour of the plasma and the resonance occurs when they have the *critical density*, n_c, given, for λ micrometres, by

$$n_c = 10^{21}\,\lambda^{-2}\,\mathrm{cm}^{-3}. \tag{1}$$

In the common situation of full ionization of a low Z material, where the atomic mass $A \approx 2Z$, the critical density n_c corresponds to a mass density

$$\rho_c = 3.3\times 10^{-3}\,\lambda^{-2}\,\mathrm{g\,cm}^{-3},$$

as illustrated in figure 1; ρ_c is thus generally small relative to solid material density.

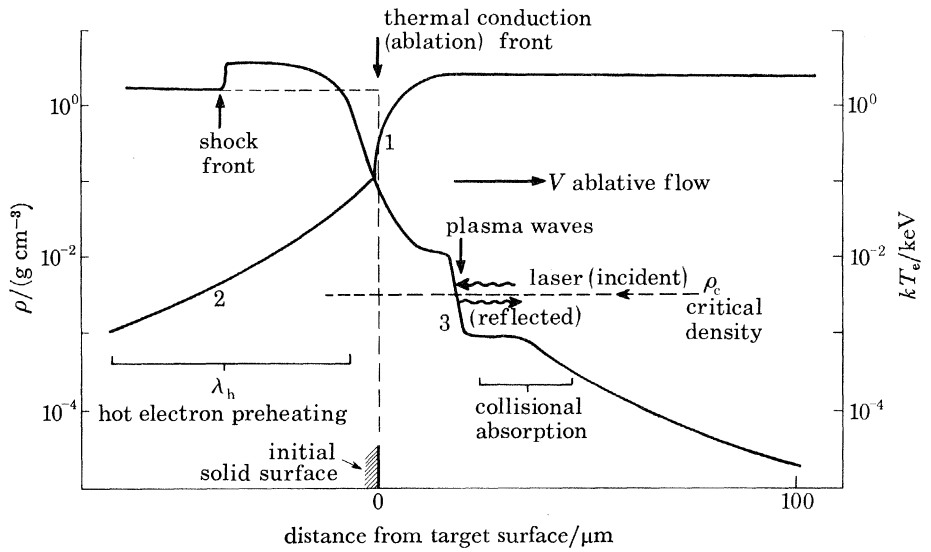

FIGURE 1. Schematic presentation for a laser-produced plasma of the variation of the plasma density, ρ, and electron temperature, T_e, with distance from the initial position of a solid surface in vacuum. Particular features of the plasma discussed in the text are labelled and the conditions of irradiation producing such a plasma are defined in the text. 1, Ablation pressure; 2, preheat pressure; 3, light pressure.

(*b*) *Absorption*

The simplest form of absorption of laser photons by the plasma is inverse Bremsstrahlung in which an electron in binary collision with an ion absorbs a photon.

The absorption coefficient, K, may be written

$$K = \frac{10^6\rho^2 Z\lambda^2}{(kT_e)^{\frac{3}{2}}\,(1-\rho/\rho_c)^{\frac{1}{2}}}\ \mathrm{cm}^{-1}, \tag{3}$$

where kT_e is in kiloelectronvolts, and expresses the fact that the binary collision probability scales as $Z\rho^2 T_e^{-\frac{3}{2}}$. It follows from (3) that most absorption in a plasma of the structure shown in figure 1 occurs where the density is greatest (i.e. $\rho \to \rho_c$). Thus, from (2) and (3), K_{max} scales as $Z\lambda^{-2}T^{-\frac{3}{2}}$ and therefore low Z, long wavelength and high temperature (resulting from high intensity) lead to poor efficiency of collisional absorption. As a result, laser radiation typically reaches the critical density with relatively little loss of intensity due to collisional absorption.

Several resonant processes involving the laser electromagnetic wave and plasma waves can then develop. The most effective of these is resonance absorption (Friedberg *et al.* 1972). Solution of Maxwell's equations shows that p-polarized light incident on a steeply rising plasma density at a few degrees from normal incidence has a singularity in the magnitude of the oscillatory electric field vector along the normal to the surface at the point of reflexion. The oscillatory field resonantly drives an electron plasma wave to very large amplitude. Wave damping occurs by collisionless 'wave breaking' or 'Landau damping'. The main feature of the damping is that a minority of the plasma electrons move through the oscillatory plasma wave electric field rapidly enough to experience continuous acceleration and thus acquire an energy of the order Eel, where E is the resonant electric field and l its extent in space. Under optimum conditions, up to 40% absorption may occur by resonance absorption, and the energy thus absorbed is transferred to a small percentage of the plasma electrons whose 'temperature' is up to 10 times higher than the background plasma temperature. These electrons are commonly described as 'hot electrons', with T_h being the 'hot electron temperature'. It is characteristic of absorption occurring through excitation of plasma waves that 'hot electrons' are produced in contrast to collisional absorption, which heats all electrons to a single temperature (Forslund *et al.* 1977).

Stimulated scattering, particularly Brillouin back scattering from acoustic waves in the plasma, prevents laser energy from reaching the region of efficient absorption. A long path length at high intensity in isothermal plasma enhances the effect, which is therefore more pronounced for longer laser pulses and larger radius targets. It has been an important but not totally dominant process in experiments to date, but since it could theoretically backscatter almost 100% of the incident laser radiation it is of considerable interest for proposed longer pulse larger target laser fusion experiments (Phillion *et al.* 1977).

Typically about half the incident laser radiation is absorbed, with most absorption at high intensities occurring through resonance absorption. The non-absorbed radiation is either reflected from the critical surface or 'reflected' by stimulated backscattering (Shay *et al.* 1978).

The objectives of much current research are to establish in detail the relative roles of the various absorption processes over a wide range of experimental parameters such as laser intensity, pulse duration, wavelength, angle of incidence, polarization, target composition and geometry. The relative significance of stimulated scattering is a particular area of uncertainty and of interest at present.

(*c*) *Energy transport*

Absorption transfers energy to plasma electrons at subcritical density. Diffusion of the heated electrons carries energy away from the point of absorption and in particular into plasma of greater than critical density. The thermal diffusion process, like collisional absorption, is governed by the characteristics of charged particle collisions (see, for example, Spitzer 1956)

PHILOSOPHICAL TRANSACTIONS OF THE ROYAL SOCIETY A MATHEMATICAL, PHYSICAL & ENGINEERING SCIENCES

whose cross section scales with energy ϵ as ϵ^{-2}. The thermal diffusivity η, governing heat conduction by electrons, scales as $T_e^{\frac{5}{2}} \rho^{-1} Z$.

The ρ^{-1} scaling of η leads to almost constant temperature in the subcritical density plasma because of rapid thermal diffusion. At supercritical density, where ρ increases, η decreases. As temperature also decreases in the thermal conduction front, the $T^{\frac{5}{2}}$ dependence cuts off the diffusion process, leading to the formation of a steep heat conduction front (see, for example, Zeldovich & Raizer 1968) as illustrated in figure 1.

The above diffusive description of heat conduction is only valid where the electron mean free path, λ_e is small compared with the scale length for temperature change, $T(\mathrm{d}x/\mathrm{d}T)$. When $\lambda_e > T(\mathrm{d}x/\mathrm{d}T)$, the heat flux cannot exceed the free streaming flux limited value $n_e(\frac{3}{2}kT_e)\, v_{et}$, where v_{et} is the mean electron thermal velocity. In fact it has been found that heat transfer in the heat front is inhibited to a level about one-thirtieth that predicted by the above Spitzer conductivity and free streaming flux limited description (Malone *et al.* 1975). The reasons for this are not clear at present, though heat flux driven acoustic wave turbulence (Manheimer 1976) and thermoelectrically generated megagauss magnetic fields (Key 1975) have been invoked as causing the inhibition.

The above description refers to the transfer of energy by the thermal electrons. The hot electrons, because $T_h \approx 10\, T_e$ and because λ_h scales as ϵ^2 and thus as T_h^2, have $\lambda_h \gg \lambda_e$ so that their effect on energy transport is close to the free streaming flux limit. They may penetrate through many micrometres of solid material, creating a preheating of the solid which diminishes with distance as shown in figure 1 (see, for example, Kilkenny *et al.* 1979). The ratio of depths of penetration into the solid of the heat front and of the hot electron preheating is a function of laser intensity but can be quite large (e.g. 0.1 μm : 20 μm at *ca.* 2×10^{15} W cm^{-2}; Kilkenny *et al.* 1979). Furthermore, the proportion of the absorbed laser energy that goes into each form of energy transport is variable, with fast electron preheating carrying the bulk of the energy at high intensities (Kilkenny *et al.* 1979).

In the study of energy transport the current areas of uncertainty relate to the mechanisms causing the apparent thermal transport inhibition and controlling the relative magnitude of hot electron and thermal electron energy transport. The available experimental data on these questions are limited in the parameter range that they cover, and theoretical models are at present incomplete and not fully verified by experiment.

(*d*) *Pressure*

There are three kinds of pressure of primary interest in laser-produced plasmas. The smallest in magnitude is *light pressure*, P_L, due to the laser radiation. This can be estimated from the momentum of a photon $P(\lambda) = h/\lambda$ and the rate of momentum transfer by absorption of $n(\lambda)$ photons cm^{-2} s^{-1}. Expressing $n(\lambda)$ in terms of intensity I(W cm^{-2}), P_L can be written

$$P_L = I/c = 3 \times 10^{-16}\, I\,\mathrm{Mbar}\dagger. \qquad (4)$$

Megabar values of light pressure are thus seen to occur in laser-produced plasmas at *ca.* 10^{16} W cm^{-2} intensity. The main effect of the light pressure is to steepen the density gradient in the plasma flow in the vicinity of the critical density (Attwood *et al.* 1978; Raven & Willi 1979) as shown schematically in figure 1. The effect is enhanced because there is an increase of light pressure near the critical density above the value indicated by (4). This increase is of

† 1 Mbar = 10^{11} Pa.

the order $(1-\rho/\rho_c)^{-\frac{1}{2}}$ and arises from the swelling of energy density in the light wave where the refractive index and the group velocity of the wave tend to zero at the critical density. The density gradient steepening significantly modifies both absorption and energy transport and is therefore an important factor in the physics of laser produced plasmas.

Ablation pressure, P_a, is the pressure exerted at the thermal conduction front (or ablation front) shown in figure 1. The term ablation pressure is used because the pressure is associated with flow or ablation from the solid of heated plasma. The pressure is greatest where ρT_e is greatest, i.e. at the ablation front, where thermal conduction has raised the temperature of material of several times the critical density to a temperature comparable with the ablation plasma temperature, T_a, in the near isothermal flow region in figure 1. The inhibition of thermal conduction discussed above is important because it reduces P_a.

Ablation pressure is exerted by plasma at densities much less than solid density and has the effect of driving a compression or shock wave into the solid, as shown in figure 1. Since a low-density medium is accelerating a high-density medium, there is instability of the Rayleigh–Taylor type at the interface, which may be an important factor in using ablative compression to produce high density plasma in laser fusion research as is considered below (Freeman *et al.* 1977).

Preheating of the solid by hot electrons can raise the pressure in the solid to high levels. This *hot electron preheat pressure* P_h is exerted by material at solid density and low temperature relative to the ablation plasma, as shown in figure 1. Its magnitude relative to P_a increases with increasing laser intensity, as hot electron energy transport becomes dominant and pressures comparable with P_a are generated for $I\lambda^2 > 10^{15}$ W cm^{-2} μm^2. The hot electron temperature and thus the relative significance of hot electron energy transport is thought to be governed by the value of $I\lambda^2$ as discussed in § (*e*) below.

The effect of preheating in, for example, thin-walled spherical shell targets (glass microballoons) of wall thickness Δr less than the preheat depth λ_h is to cause the explosion of the wall and consequent compression of gas in the microballoon. The gas, being also preheated, is compressed on a high adiabat to give a relatively high final temperature and low final density in such 'exploding pusher' targets. In laser fusion experiments, D_2+T_2 densities of 0.2 g cm^{-3} and ion temperatures up to $kT_i \approx 10$ keV have been obtained in this way (Lerche *et al.* 1977; Key *et al.* 1979*a*).

(*e*) *Ablatively driven implosions*

The exploding pusher mode of compression cannot yield the very high compressed density that is in principle obtainable by isentropic compression (i.e. compression without preheating). Ablation pressure, being generated behind a sharply defined front, can in principle be used to drive the implosion of thin spherical shells of material to create plasma densities of the order of 1000 g cm^{-3}. This is both a fascinating research possibility and an important technological possibility, since it would permit efficient small-scale inertially confined thermonuclear burning of D_2+T_2. The essential point here is that the minimum mass of fuel in which a nucleus experiences of sufficient number of collisions to ensure thermonuclear fusion scales as ρ^{-2} (Emmett *et al.* 1974).

An estimate of ablation pressure can be made by assuming that the ablative flow occurs at the plasma sound velocity, v_s, and at the critical density, ρ_c.

The sound velocity is approximately (with kT_a in kiloelectronvolts)

$$v_s \approx (P_a/\rho_a)^{\frac{1}{2}} \approx 2\times 10^7 (kT_a)^{\frac{1}{2}} \text{ cm s}^{-1}. \quad (5)$$

The kinetic and thermal energy contents of such a flow are similar in magnitude so that half the absorbed laser intensity, I_a, can be equated to the flux density of kinetic energy,

$$0.5\, I_a = \rho_a v_a(\tfrac{1}{2}v_a^2), \tag{6}$$

and the ablation pressure can be estimated from the momentum flux density,

$$P_a = \rho_a v_a(v_a) = 200\ (I_a/10^{16})^{\frac{2}{3}}\, \lambda^{-\frac{2}{3}}\ \text{Mbar}. \tag{7}$$

It may be seen at this point that the ratio P_a/P_L scales as $(I\lambda^2)^{-\frac{1}{3}}$ and it is also readily shown that $P_a/P_L \approx (v_{et}/v_{osc}$, where v_{osc} is the oscillatory velocity of a free electron in the laser e.m. wave. The relative importance of laser-driven plasma waves depends in general on v_{et}/v_{osc} and thus on $(I\lambda^2)$, as noted above. It has been found experimentally, for example, that in experiments comparing $\lambda = 10.6$ μm and 1.06 μm the same value of T_h is obtained for the same value of $I\lambda^2$ (Forslund *et al.* 1977).

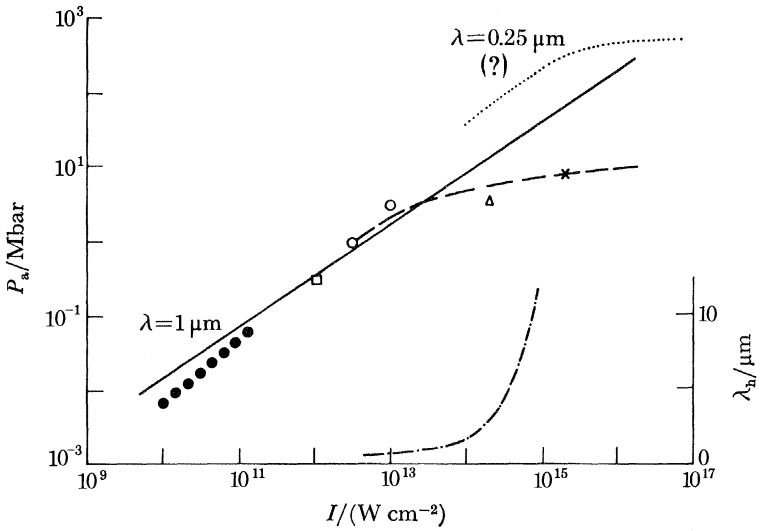

FIGURE 2. The solid line is for $\lambda = 1$ μm from the analytic model (see equation (7)) and the data points are collected from various experimental sources, also for $\lambda = 1$ μm. The broken line indicates the experimental sources, also for $\lambda = 1$ μm. The broken line indicates the experimentally observed saturation in the ablation pressure increase. The dotted line is a speculative indication of how this saturation might occur for $\lambda = 0.25$ μm, following the simple arguments in the text. The dot-dash line shows the approximate magnitude of λ_h in solid polymer as a function of laser intensity.

Figure 2 shows a comparison of analytical model and experimental intensity scaling of P_a for $\lambda = 1.06$ μm together with an indication of the intensity scaling of λ_h. It is seen that where λ_h becomes large enough for significant penetration of hot electrons into the solid, the rate of increase of P_a with I saturates markedly.

This increase of preheating and fall-off of ablation pressure is a major problem for ablative implosion experiments and has prompted considerable interest in the question of whether shorter wavelength lasers can give larger ablation pressure for a given intensity (equation (7)) and/or a higher intensity threshold for the hot electron effects in figure 2 because of $I\lambda^2$ scaling of these effects. This question remains somewhat open at present.

It has also been suggested that the apparently deleterious hot electrons, so readily produced by 10.6 μm CO_2 lasers, may be able to drive high density compressions through the preheat

pressure P_h in targets designed to screen the compressed gas from preheating. Thus $\lambda = 10.6$ μm may be satisfactory at one extreme and $\lambda < 1.06$ μm is being considered at the other.

(*f*) *A 'rocket' model for ablative implosions*

Despite the above qualifying remarks, ablative implosion is still regarded as the simplest way to achieve high compressed density. The requirement in this process is to produce an implosion velocity giving the material sufficient kinetic energy to do the essential compressive work. An implosion velocity of 3×10^7 cm s^{-1} gives the minimum kinetic energy that could yield 1000 g cm^{-3} in an isotropic compression of Fermi degenerate plasma (Emmett *et al.* 1974).

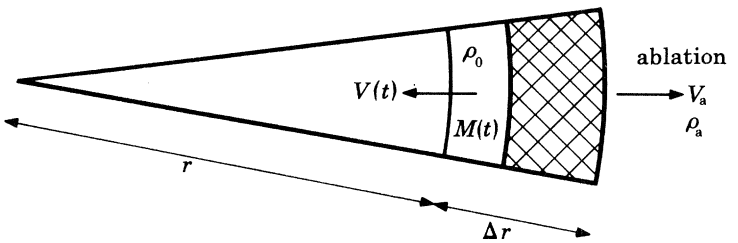

FIGURE 3. Schematic representation of part of a spherical shell target of initial density ρ_0 undergoing ablative acceleration. The shaded part of the shell is assumed to be removed by ablation as the implosion proceeds through a distance r.

The velocity obtained by ablative acceleration of a shell of thickness Δr and radius r can be estimated with reference to figure 3, from the simple rocket analogy in which the mass ablation rate per unit area $M(t) = \rho_a v_a$ and the equation of motion of the residual mass per unit area $M(t)$ is

$$M(t)\,\dot{v}(t) = \rho_a v_a^2 = \dot{M}(t)\,v_a, \tag{8}$$

with the simple solution

$$\frac{v(t)}{v_a} = \ln\left(\frac{M_0}{M(t)}\right) \to \lim_{\Delta M \to 0} \Delta M/M. \tag{9}$$

The efficiency of converting absorbed energy into 'payload' kinetic energy is easily shown to be $\lim_{\Delta M \to 0} \Delta M/M$.

Thus, with ablation of most of the shell thickness a final velocity about equal to v_a is obtainable with reasonable hydrodynamic efficiency. Values of v_a of a few tens of millions are typically obtained at $I\lambda^2 \geqslant 10^{14}$ W cm^{-2} μm^2, indicating the general feasibility of ablative acceleration to the velocity discussed above.

It is interesting to note that if $I\lambda^2$ is constant for constant hot electron effects, then v_a is constant from (5), (6) and (7) above. Then if $\Delta M/M_0$ is constant for optimum efficiency, $v(t)$ is constant, suggesting no wavelength dependence of attainable implosion velocity. However, it also follows from the rocket model in figure 3 and equation (8) that with these constraints,

$$r/\Delta r \approx \rho_0/\rho_a, \tag{10}$$

where ρ_0 is the solid shell density. Since the Rayleigh–Taylor instability growth is maximum for a perturbation wavelength equal to the shell thickness and the growth rate $\gamma \approx \{K\dot{v}(t)\}^{\frac{1}{2}}$ for perturbation wave number K and acceleration $\dot{v}(t)$, the total growth in acceleration to a given final velocity scales as $\exp(r/\Delta r)^{\frac{1}{2}}$. Thus large values of $r/\Delta r$ are expected to lead to unstable break-up of the imploding shell.

PHILOSOPHICAL TRANSACTIONS OF THE ROYAL SOCIETY A MATHEMATICAL, PHYSICAL & ENGINEERING SCIENCES

Equation (10) suggests the use of low ρ_0 or high ρ_a to counter this problem, and if $\rho_a \approx \lambda^{-2}$, short wavelengths are desirable, unless ρ_a can be raised effectively to solid density by using hot electron preheat pressure generated by long wavelength laser.

These unresolved problems are at the centre of vigorous experimental and theoretical study at present and provide a considerable intellectual challenge whose practical significance may also be very high if a solution to the controlled thermonuclear fusion problem is found in this way.

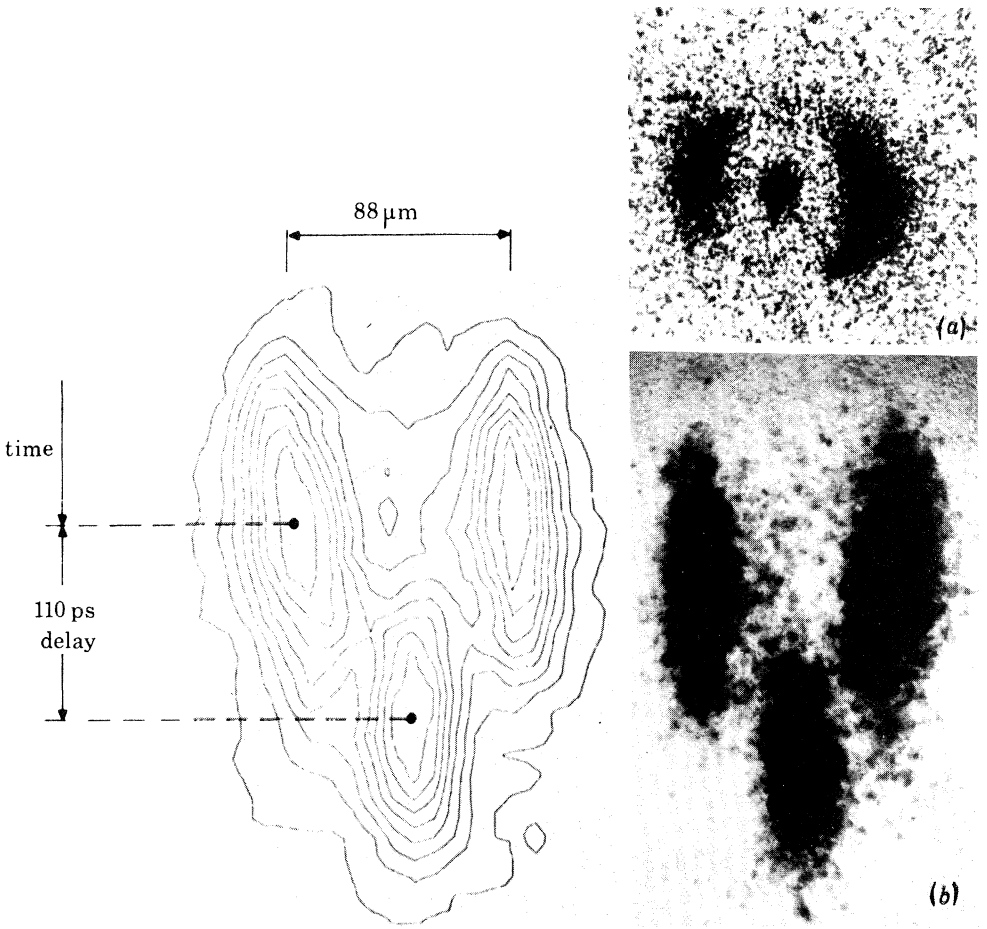

FIGURE 4. (*a*) Static X-ray pinhole camera image; (*b*) streaked X-ray pinhole camera image with isodensity contour representation of the streaked image. The target was a glass microballoon of 88 μm diameter and 0.88 μm wall thickness, filled with D_2+T_2 gas at 10 bar pressure and irradiated with 15 J of $\lambda = 1.06$ μm laser energy in 100 ps. The 110 ps implosion time is shown in the diagram.

3. ILLUSTRATIONS OF FAST TIME-RESOLVED MEASUREMENTS WITH ELECTRON OPTICAL STREAK CAMERAS ON LASER-PRODUCED PLASMAS

(*a*) *Introduction*

The close connection between the development of ultra-short laser pulses and of picosecond resolution streak cameras has been emphasized in preceding papers at this meeting. It is interesting to note that the study of plasmas produced by ultra-short laser pulses has involved a similar close connection with new developments in streak cameras arising through new diagnostic objectives.

(*b*) *X-ray streak camera observations*

The development of X-ray streak cameras (Bradley *et al.* 1975) is the most striking example of this. The first application of X-ray cameras to the study of compression by lasers was in the measurement of implosion velocity in exploding pusher targets, in which both the ablation plasma and the implosion core are intense sources of 1 keV X-ray emission (Key *et al.* 1979*b*; Attwood *et al.* 1977). Figure 4 illustrates such a measurement where the implosion time of the target is only 100 ps.

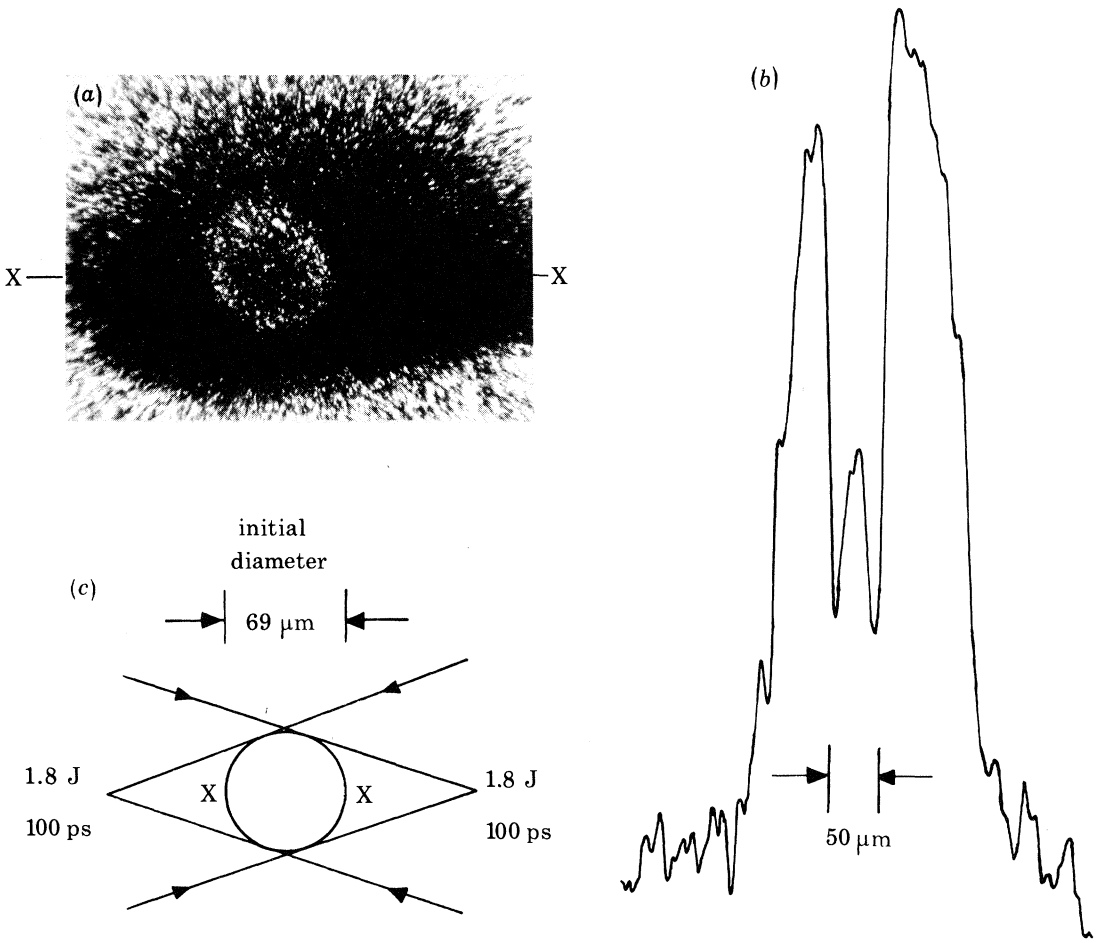

FIGURE 5. Pulsed X-ray shadowgraph image (*a*) and densitometer trace (*b*) of absorption zone along XX, recorded with a 100 ps pulse of X-ray emission from a laser-produced plasma 250 ps after irradiation of the glass microballoon target. The target (*c*) was of 69 μm diameter, 1.3 μm glass wall thickness and filled with 87 bar Ne. It was irradiated at 5×10^{14} cm^{-2} with 3.6 J in 100 ps and imploded in *ca.* 700 ps. The shadowgraph and densitometer tracing show a ringlike zone of maximum absorption associated with a dense shell of imploding material before stagnation of the implosion at the centre.

Currently there is much interest in achieving significantly higher densities by using the ablative mode of compression. This type of compression event produces a lower compression core temperature and the combination of high density and low temperature gives an implosion core whose X-ray emission is in the main too soft to escape from the target and too weak to measure.

PHILOSOPHICAL TRANSACTIONS OF THE ROYAL SOCIETY A MATHEMATICAL, PHYSICAL & ENGINEERING SCIENCES

A promising alternative for the study of such plasmas is the recording of X-ray shadowgraphs with an externally generated source of X-rays whose brightness significantly exceeds that of the implosion plasma. It was shown by Key *et al.* (1978) that a laser-produced plasma on a solid metal target could be used as such a pulsed X-ray source. With conditions where the *ca.* 100 ps pulsed X-ray emission was of short duration relative to the *ca.* 700 ps implosion time of a high-pressure neon-filled glass microballoon target, time-resolved X-ray shadowgraphs of the implosion were obtained whose analysis demonstrated that plasma densities *ca.* 4 g cm^{-3} had been produced in the compressed neon. Figure 5 shows an example of a pulsed X-ray shadowgraph recorded 250 ps after irradiation of the microballoon target when the structure of the imploding plasma was still that of a dense shell of glass moving into the neon gas. The dense shell is revealed by the ring like zone of peak absorption in the image and in the densitometer tracing.

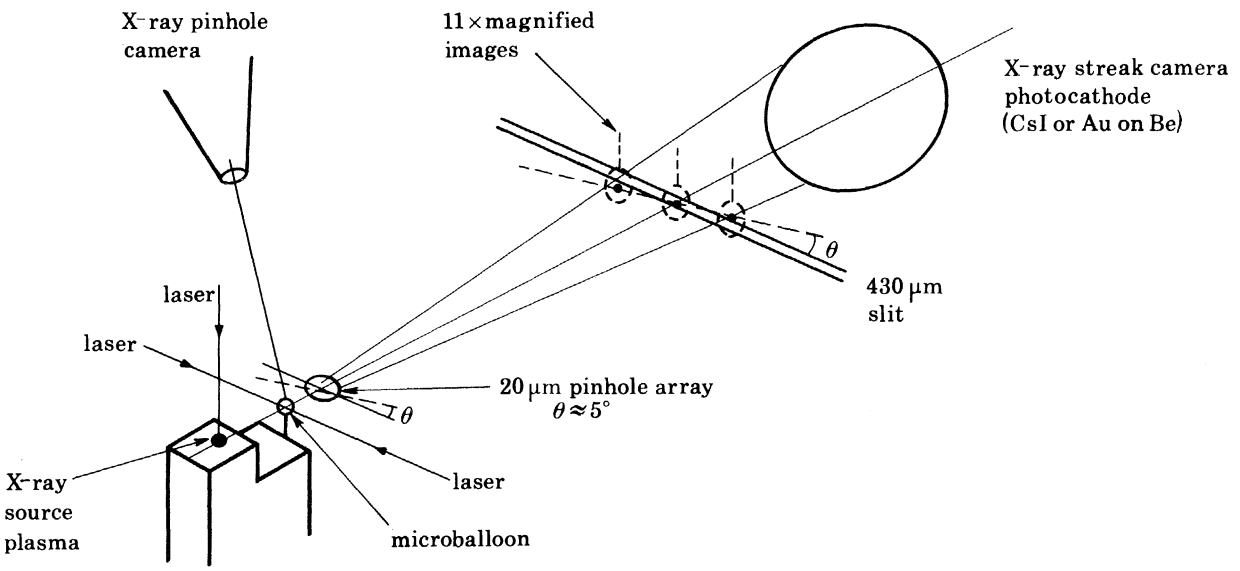

FIGURE 6. Schematic system for streak recording of X-ray shadowgraphs.

A development of this X-ray shadowgraphy method has recently been applied to the study of ablatively driven implosions. Ablative implosion was achieved with relatively thick walled microballoon targets (e.g. 2 μm of polymer on a glass substrate 1.4 μm thick). The laser intensity was low enough (*ca.* 4×10^{13} W cm^{-2} on a *ca.* 250 μm diameter target) to ensure that the hot electron preheating range λ_h was significantly less than the shell thickness Δr ($\lambda_h / \Delta r \approx 0.2$).

Laser irradiation of the target was continuous during the implosion and the implosion time was *ca.* 2 ns. Under these conditions the production of a source of X-rays for X-ray shadowgraphy by using a fraction of the laser power gave an X-ray pulse of duration similar to the implosion time and was thus unsuitable for making pulsed shadowgraph images.

The availability of X-ray streak cameras, and in particular of a system of 20 times enhanced sensitivity resulting from a newly developed low density CsI photocathodes (Key *et al.* 1979*c*) provided the means of time-resolving the shadowgraph image as shown in figure 6.

Streak records of the type shown in figure 7 were obtained. The formation of an absorption zone of *ca.* 100 μm minimum diameter after an implosion time of *ca.* 2 ns is seen in transmitted

ca. 2 keV X-rays from the auxiliary laser-produced plasma. The photograph also shows less intense emission from the ablation plasma on the microballoon target surface. There is a 1.8 ns delay in this case between the laser pulses driving the implosion and the shadowgraphy source plasma.

Analysis of the first such data is yielding some of the first evidence on the hydrodynamic stability of ablative implosions of high aspect ratio $r/\Delta r$. Figure 8 shows computed and experimentally measured time variations of absorption zone radius. It also shows the time development of $\int \gamma(t)\mathrm{d}t$, where $\gamma(t)$ is the most unstable Rayleigh–Taylor instability growth rate

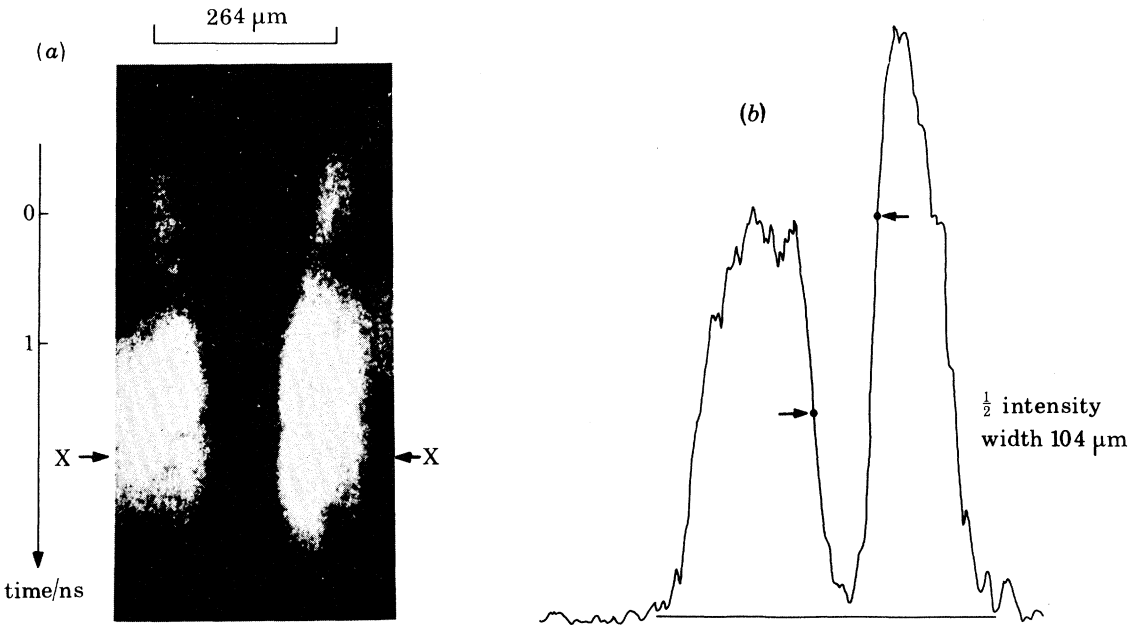

FIGURE 7. An example of a streaked X-ray shadowgraph of the implosion of a 264 μm diameter glass micro balloon with 1.4 μm glass wall thickness and a 2.0 μm polymer coating. The target was irradiated at 4×10^{13} W cm^{-2} with *ca.* 60 J in 1.6 ns and imploded in *ca.* 2 ns. The shadowgraph was recorded with 2 keV X-rays. The densitometer trace was taken along XX, 1.9 ns after peak of laser pulse.

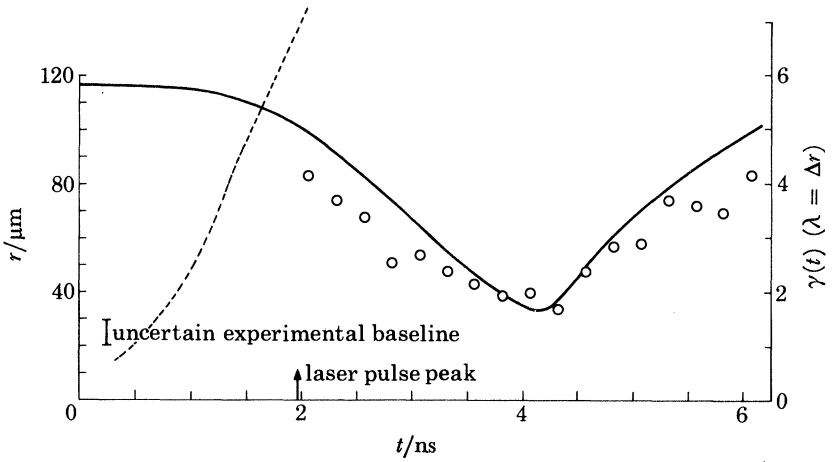

FIGURE 8. The left ordinate is the radius of the zone of opacity to X-rays ($\tau > 0.5$); the right ordinate is the exponent $\int \gamma(t)\mathrm{d}t$ of growth of the classical Rayleigh–Taylor instability of wavelength equal to the shell thickness. Solid line, computer modelling. Data points are from streaked X-ray shadowgraphy. Both show the radius for $\tau > 0.5$. Dotted line, the value of $\int \gamma(t)\mathrm{d}t$. The polymer coating was 5 μm thick.

discussed in §2*f*. The instability growth exponent $\int\gamma(t)\mathrm{d}t$ reaches large values early in the implosion process suggesting that initial surface roughness present on the targets as seen in figure 9, plate 1, may grow sufficiently to break up the imploding shell.

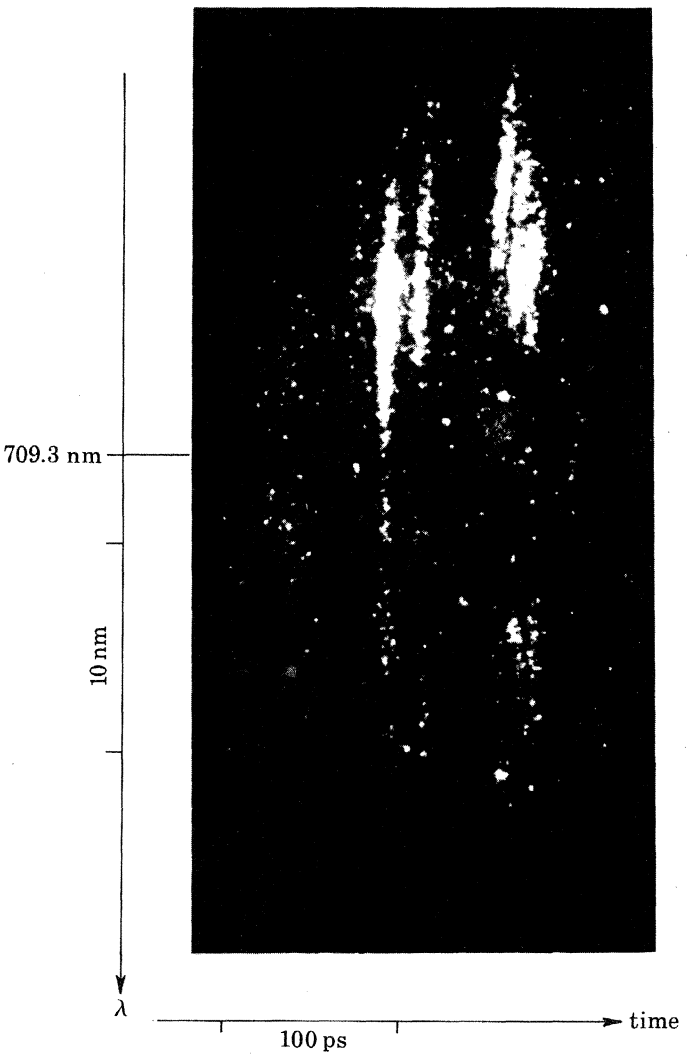

FIGURE 10. Streaked spectrum of $\frac{3}{2}\omega_L$ emission from a microballoon target irradiated at *ca.* 10^{16} W cm^{-2} with a 100 ps 1.06 μm pulse.

Preliminary evidence that this may have occurred has been obtained by comparing observed and computed features of the streak shadowgraphs. The computer simulations were made with a one-dimensional hydrodynamic model developed from the published MEDUSA code (Key *et al.* 1978). These have predicted *ca.* 10 g cm^{-3} in the implosion core and have also given computed profiles of absorption in the shadowgraph image and computed burn depth of ablation of the polymer layer on the target. The latter two features are at variance with experimental results in a manner qualitatively consistent with mixing of the glass and polymer layers in the shell due to Rayleigh–Taylor instability. The experimental shadowgraph images have a low boundary sharpness with a scale length *ca.* 30 μm which is about three times more than the instrumental resolution and computed scale length. Also, the intensity of ablation

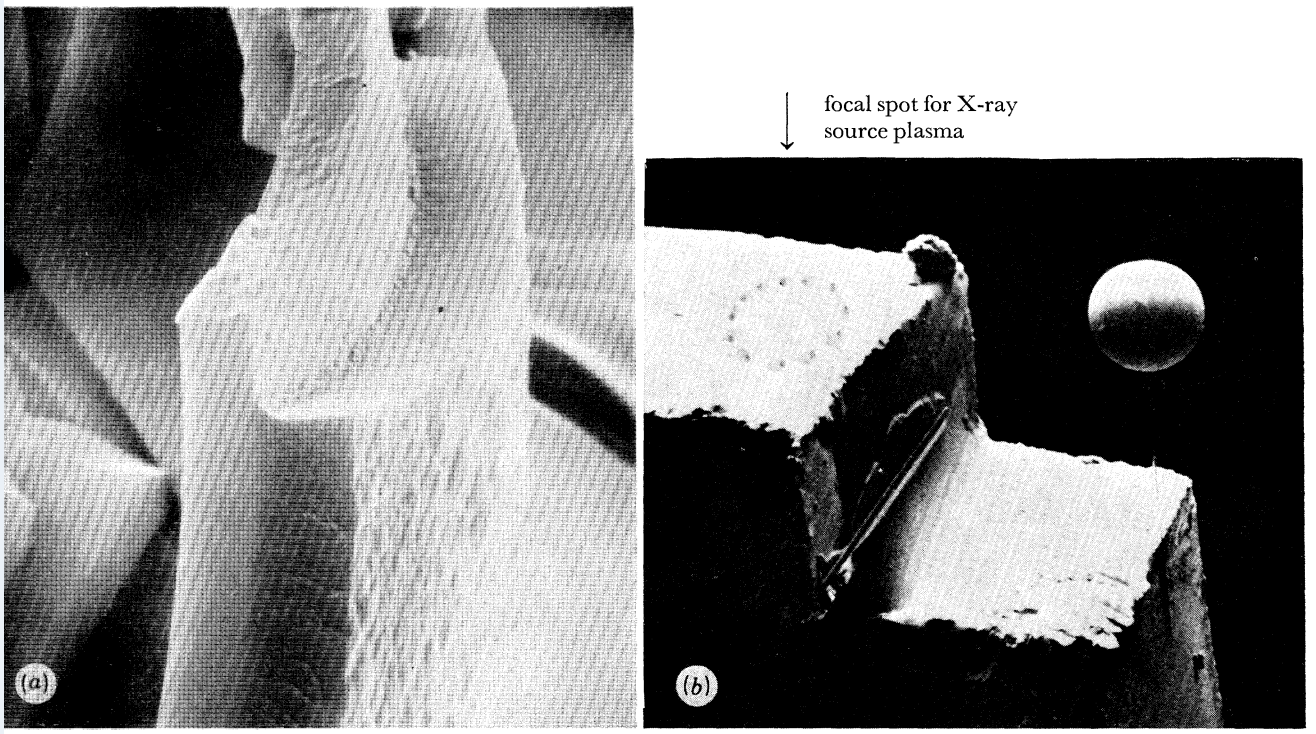

FIGURE 9. (*a*) Electron micrograph of a section of a polymer-coated target with a 2 μm polymer layer. (*b*) Electron micrograph of a polymer-coated glass microballoon mounted for X-ray streak shadowgraphy as a figure 6.

(*Facing p.* 362)

PHILOSOPHICAL TRANSACTIONS OF THE ROYAL SOCIETY A MATHEMATICAL, PHYSICAL & ENGINEERING SCIENCES

plasma X-ray emission is several times higher than for pure polymer targets and approaches that of glass targets, suggesting mixing of SiO_2 and polymer in the ablation plasma. Computed burn depths are less than the polymer layer thickness.

Further studies of this type should provide much more detailed evidence on implosion stability.

(*c*) *Visible light streak cameras*

A quite different but equally valuable application of picosecond streak camera technique is illustrated in figure 10. Here a conventional S.20 picosecond streak camera has been used to time-resolve the spectrum of $\frac{3}{2}\omega_L$ harmonic emission from 100 ps pulse laser-produced plasma at *ca.* 10^{16} W cm^{-2} (Key *et al.* 1979*c*). This harmonic is known to be associated with plasma waves generated at one-quarter of the critical density by the parametric two-plasmon decay $\omega_L \rightarrow 2\omega_p$.

Its two-peaked broad spectrum has been described in terms of processes of the type $\omega_L + \omega_p \rightarrow \omega_{\frac{3}{2}}$ and $3\omega_p \rightarrow \omega_{\frac{3}{2}}$ (Avrov *et al.* 1977), but streak recording of the spectrum as in figure 10 shows startling *ca.* 10 ps pulses of harmonic emission whose origin is still unexplained. This illustrates the value of picosecond measuring capability in recording phenomena that characterize the turbulent wave generation processes occurring in laser–plasma interactions.

(*d*) *Conclusion*

The above illustrations of the application of streak camera methods to the study of laser-produced plasmas, taken as they are from work at the Science Research Council Central Laser Facility (C.L.F.), are but a part of worldwide activity in this field. It is hoped that they give some indication both of the contribution of the C.L.F. to the subject as a whole and of the importance of time resolution techniques in the study of laser-produced plasmas.

I am grateful to many colleagues at Queen's University, Belfast, and at the S.R.C. Central Laser Facility for stimulating scientific discussion and for the provision of the illustrative experimental results presented in this paper.

References (Key)

Attwood, D. T., Coleman, L. W., Boyle, M. J., Larsen, J. T., Phillion, D. W. & Manes, K. R. 1977 *Phys. Rev. Lett.* **38**, 282.

Attwood, D. T., Sweeney, D. W., Auerbach, J. M. & Lee, P. H. Y. 1978 *Phys. Rev. Lett.* **40**, 184.

Avrov, A. I., Bychenkov, V. Y., Krokkin, O. N., Pustalov, V. V., Shikanov, A. S., Rupasov, A. A., Silin, V. P., Skliskov, G. V. & Tikkonchuk, V. T. 1977 *Soviet Phys. JETP* **45**, 3.

Bradley, D. J., Roddie, A. G., Sibbett, W., Key, M. H., Lamb, M. J., Lewis, C. L. S. & Sachsenmaier, P. 1975 *Optics Commun.* **15**, 231.

Emmett, J. L., Nuckolls, J. & Wood, L. 1974 *Scient. Am.* **230** (6), 24.

Forslund, D. W., Kindel, J. M. & Lee, K. 1977 *Phys. Rev. Lett.* **39**, 284.

Freeman, J. R., Clauser, M. G. & Thompson, J. L. 1977 *Nucl. Fusion* **17**, 223.

Friedberg, J. P., Mitchell, R. W., Morse, R. L. & Rudsinski, L. I. 1972 *Phys. Rev. Lett.* **28**, 795–799.

Key, M. H. 1978 *Nature, Lond.*, **226**, 210–211.

Key, M. H. *et al.* 1979*c* *Rutherford Laboratory Report* no. RL 79 014.

Key, M. H., Lamb, M. J., Lewis, C. L. S., Moore, A. & Evans, R. G. 1979*b* *Appl. Phys. Lett.* **34**, 550.

Key, M. H., Lewis, C. L. S., Lunney, J. G., Moore, A., Hall, T. A. & Evans, R. G. 1978 *Phys. Rev. Lett.* **41**, 1467.

Key, M. H., Lunney, J. G., Ward, J. M., Evans, R. G. & Rumsby, P. T. 1979*a* *J. Phys.* B **12**, L213.

Kilkenny, J. D., Hares, J., Key, M. H. & Lunney, J. G. 1979 *Phys. Rev. Lett.* **42**, 1216–1218.

Lerche, R. A., Coleman, L. W., Houghton, J. W., Speck, D. R. & Storm, E. K. 1977 *Appl. Phys. Lett.* **31**, 645.

Malone, R. C., McRory, R. L. & Morse, R. L. 1975 *Phys. Rev. Lett.* **34**, 721.
Manheimer, W. M. 1976 *Phys. Fluids* **20**, 265.
Phillion, D. W., Kruer, W. L. & Rupert, V. C. 1977 *Phys. Rev. Lett.* **39**, 1529.
Raven, A. & Willi, O. 1979 *Phys. Rev. Lett.* **43**, 278
Shay, H. D. *et al.* 1978 *Phys. Fluids* **21**, 1634.
Spitzer, L. J. 1956 *Physics of fully ionised gases*. New York: Interscience.
Zeldovich, Y. B. & Raizer, Y. P. 1968 *Physics of shock waves and high temperature hydrodynamic phenomena*, vol. 1. Academic Press.

Discussion

C. YAMANAKA (*Institute of Laser Engineering, Osaka University, Japan*). Fluid instability in compression was discussed in Dr Key's talk. What is the most definite experimental result giving evidence of such instability? Is the observation of aluminium X-ray line emission from the implosion core of aluminium-coated targets sufficient evidence to prove the occurrence of the instability?

M. H. KEY. We have in the past reported the observation of aluminium X-ray line emission from the implosion core in aluminium-coated 'exploding pusher' targets. This is surprising since such targets are not expected theoretically to be subject to Rayleigh–Taylor instability. The experimental evidence has been carefully checked however, and the aluminium is observed in the implosion core. The process could be associated with non-uniform two-beam irradiation of the microballoon.

Ablative implosions with high aspect ratio are expected theoretically to be unstable as shown in my talk, and the best evidence of the instability that we have to date is from streaked X-ray shadowgraphy experiments in which two anomalous observations were recorded:

(*a*) Polymer-coated glass targets had anomalously intense 2–3 keV X-ray emission due to SiO_2 in the ablation plasma. The polymer layer was too thick for this to be explained by ablation front burn depth.

(*b*) The boundary of the zone of absorption was about three times more diffuse than the instrumental resolution limit and computer-simulated sharpness. This could be explained by SiO_2 mixing with the ablating polymer.

This evidence is consistent with Rayleigh–Taylor instability and cannot easily be explained otherwise, but is still not very direct evidence.

PHILOSOPHICAL TRANSACTIONS OF THE ROYAL SOCIETY A MATHEMATICAL, PHYSICAL & ENGINEERING SCIENCES

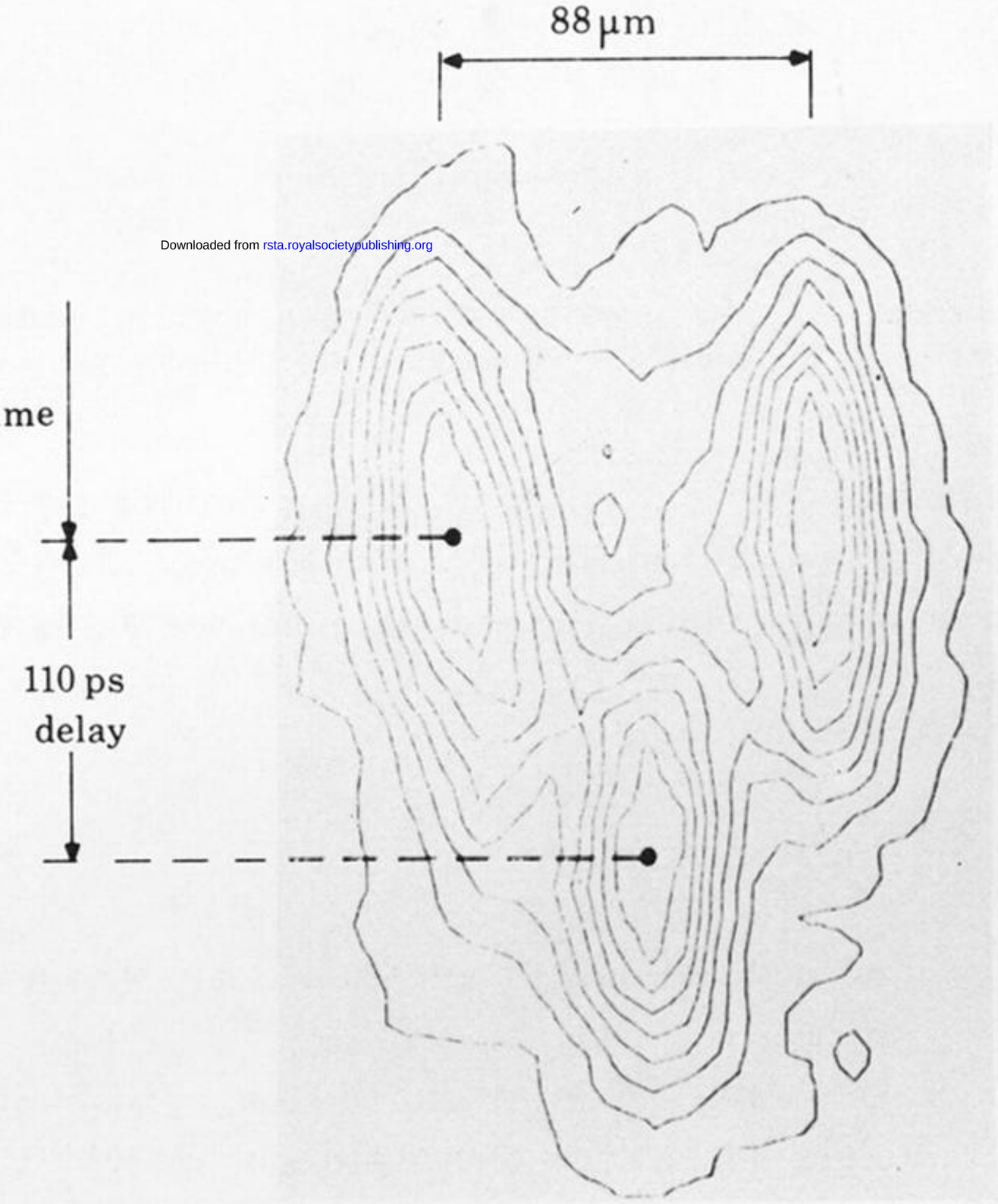

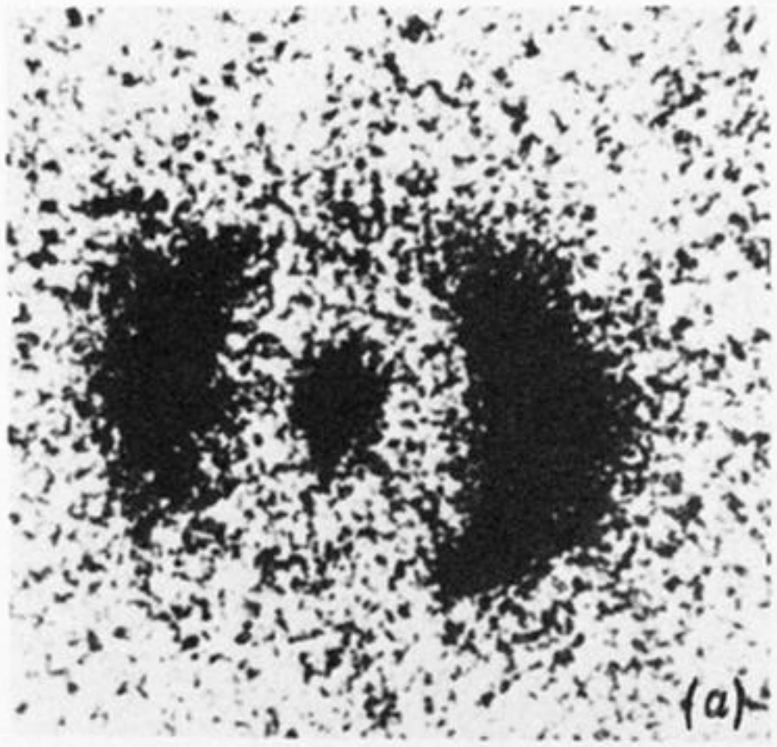

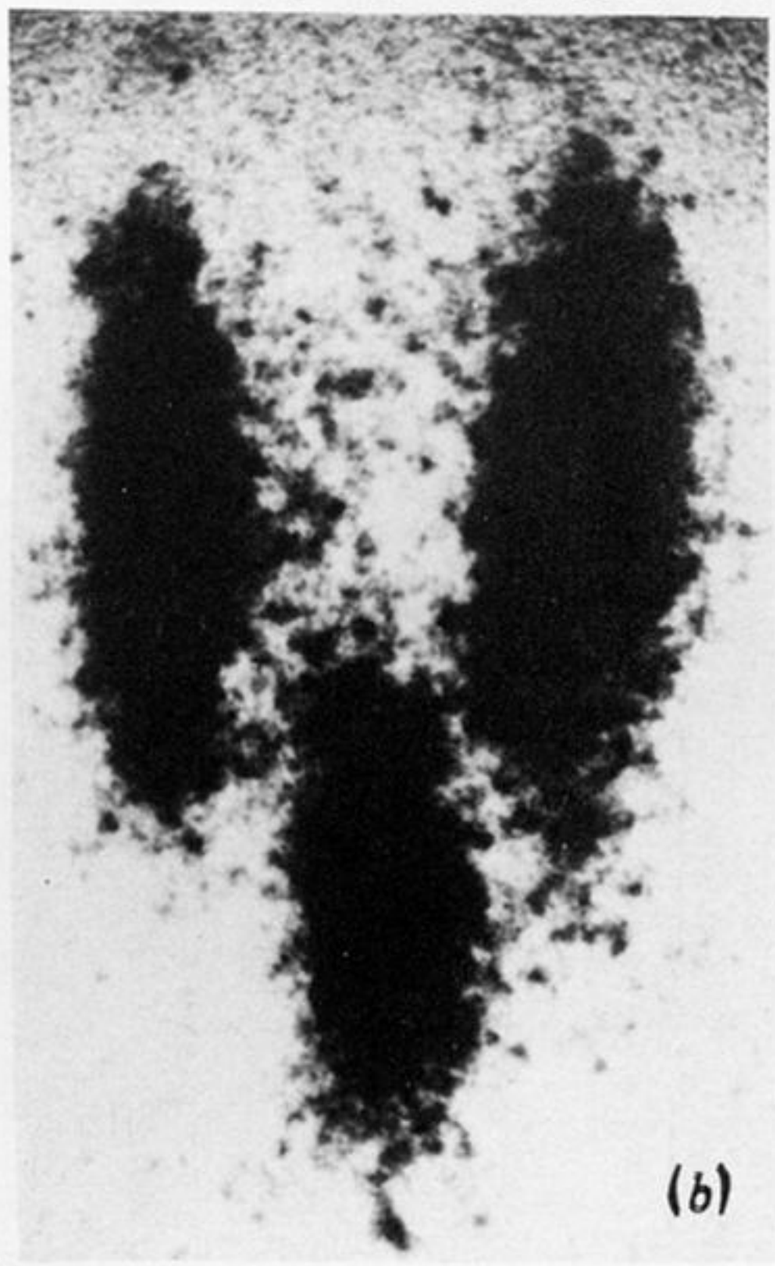

FIGURE 4. (*a*) Static X-ray pinhole camera image; (*b*) streaked X-ray pinhole camera image with isodensity contour representation of the streaked image. The target was a glass microballoon of 88 μm diameter and 0.88 μm wall thickness, filled with D_2+T_2 gas at 10 bar pressure and irradiated with 15 J of $\lambda = 1.06$ μm laser energy in 100 ps. The 110 ps implosion time is shown in the diagram.

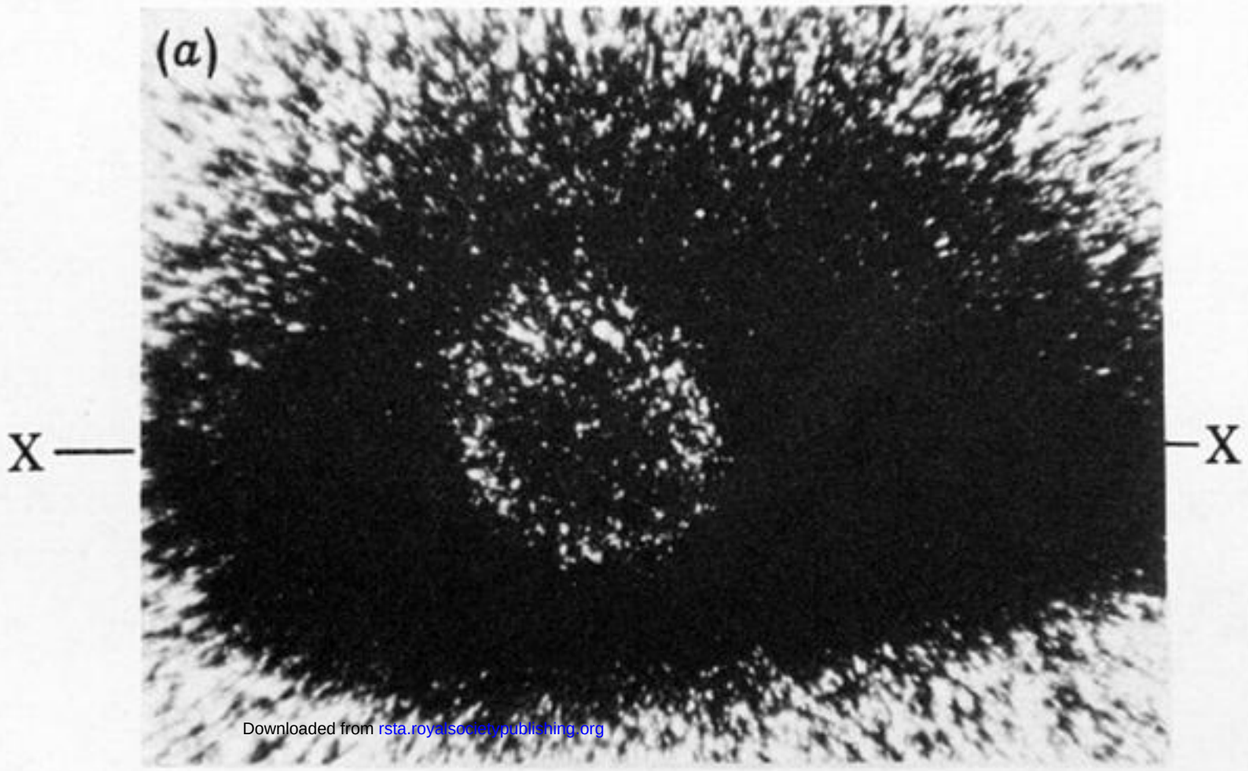

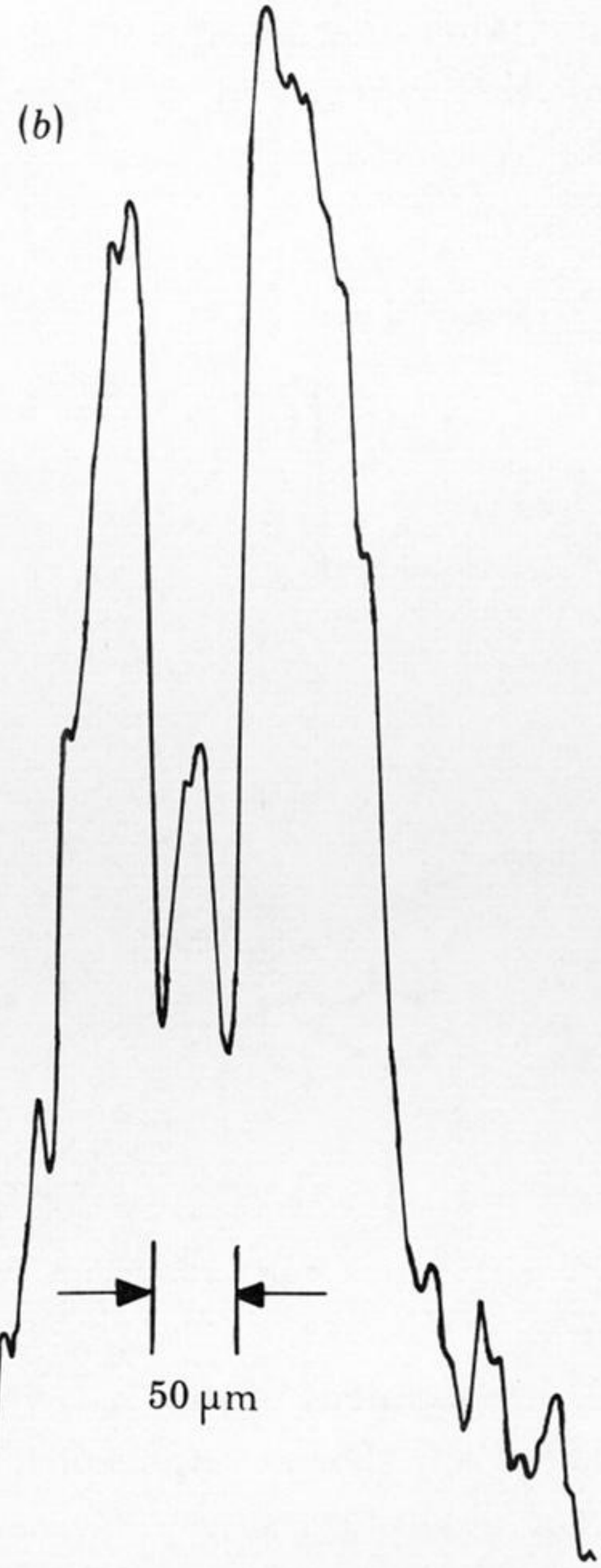

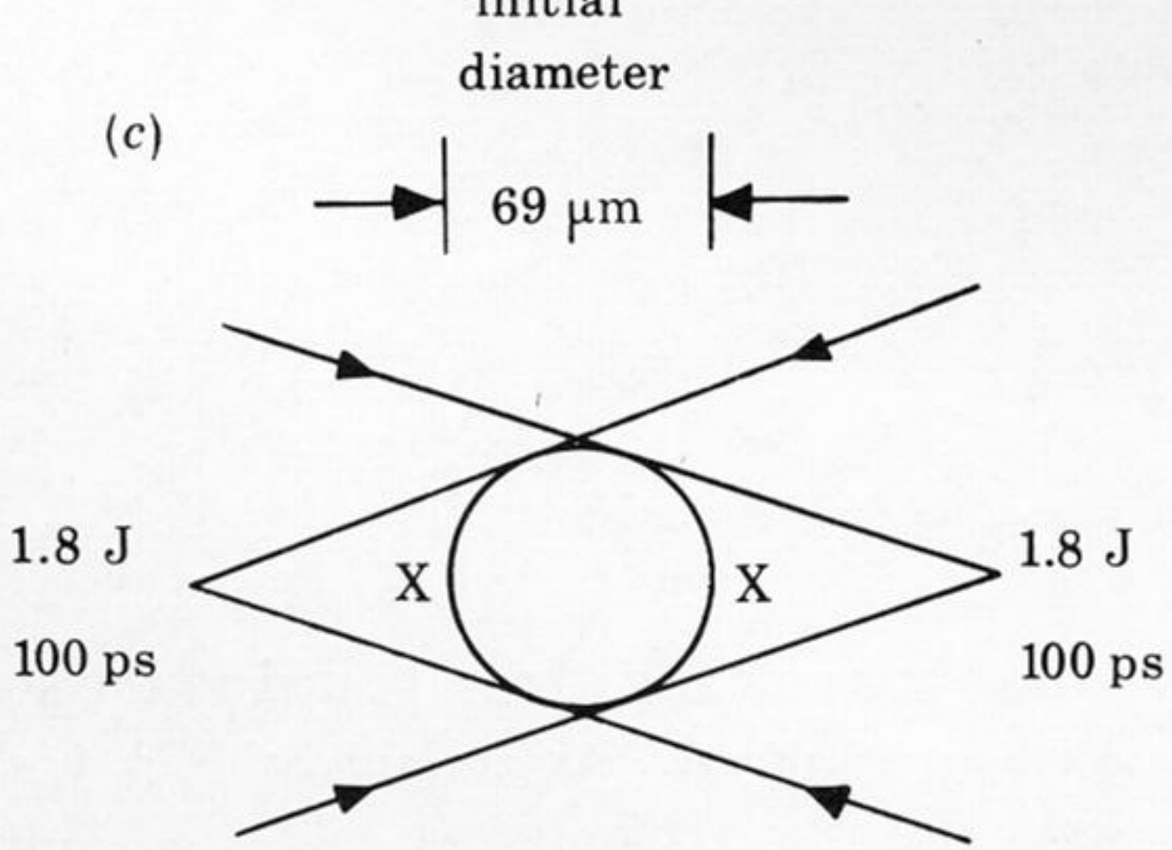

FIGURE 5. Pulsed X-ray shadowgraph image (*a*) and densitometer trace (*b*) of absorption zone along XX, recorded with a 100 ps pulse of X-ray emission from a laser-produced plasma 250 ps after irradiation of the glass microballoon target. The target (*c*) was of 69 μm diameter, 1.3 μm glass wall thickness and filled with 87 bar Ne. It was irradiated at 5×10^{14} cm^{-2} with 3.6 J in 100 ps and imploded in *ca.* 700 ps. The shadowgraph and densitometer tracing show a ringlike zone of maximum absorption associated with a dense shell of imploding material before stagnation of the implosion at the centre.

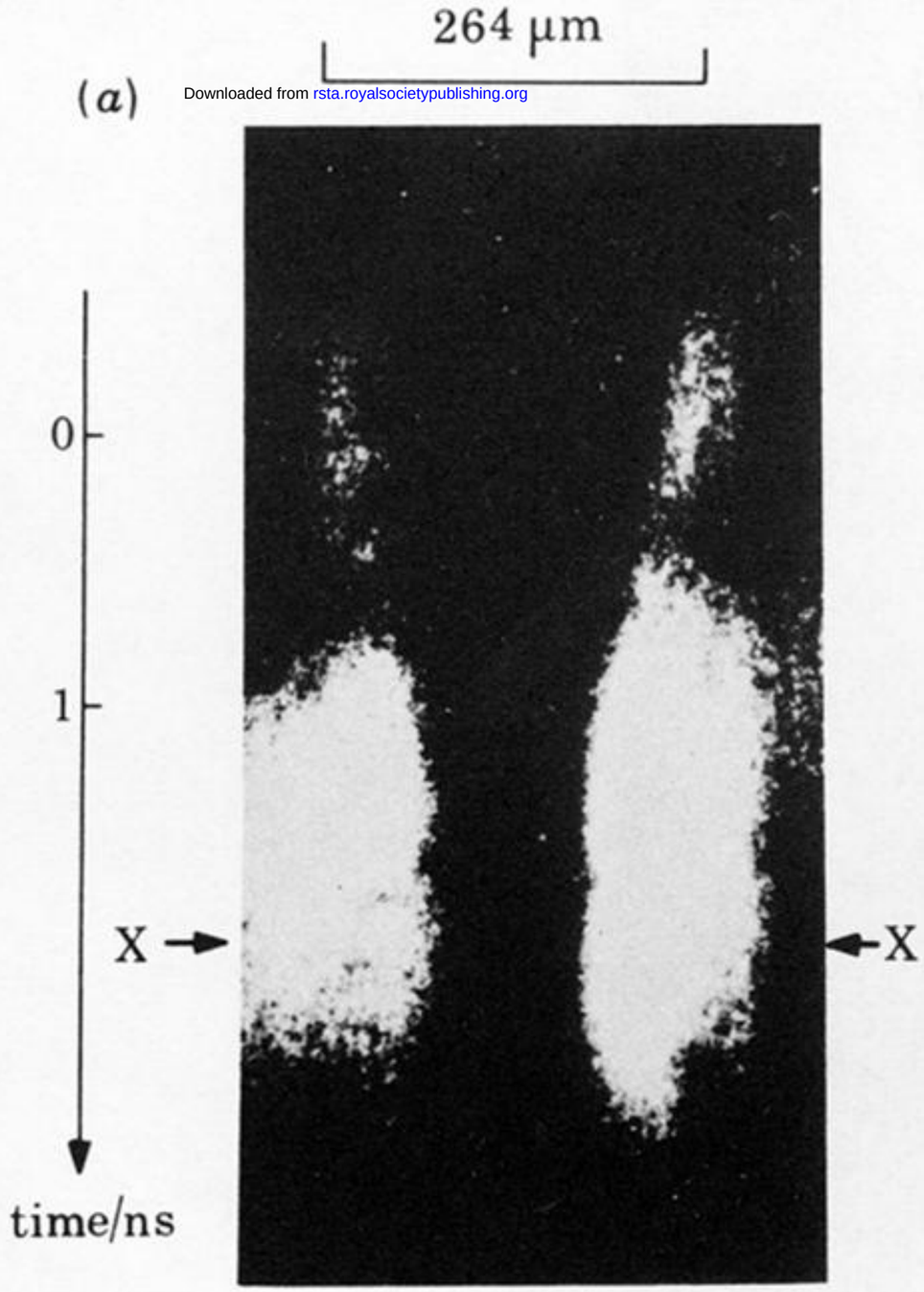

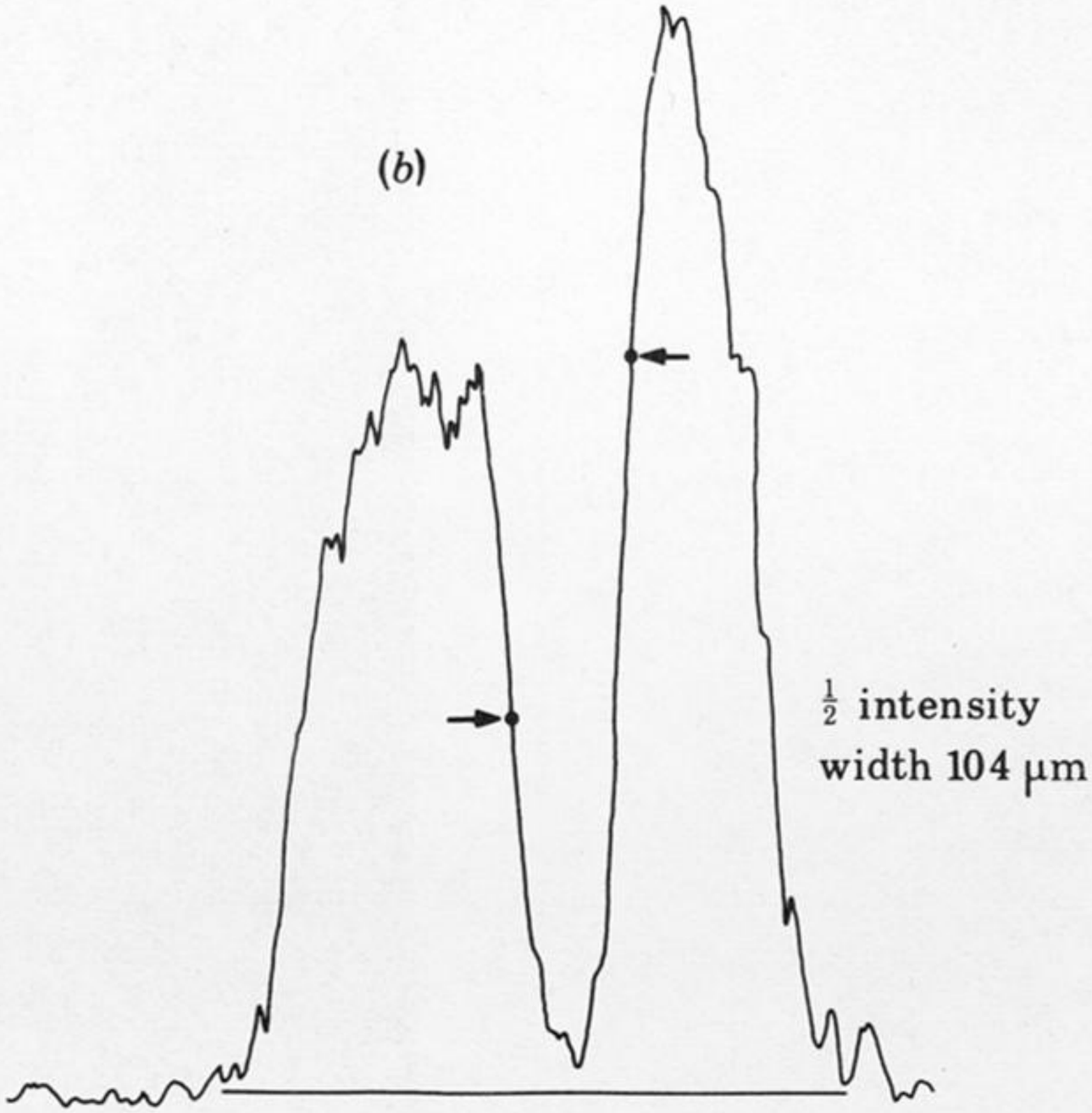

FIGURE 7. An example of a streaked X-ray shadowgraph of the implosion of a 264 μm diameter glass micro balloon with 1.4 μm glass wall thickness and a 2.0 μm polymer coating. The target was irradiated at 4×10^{13} W cm^{-2} with *ca.* 60 J in 1.6 ns and imploded in *ca.* 2 ns. The shadowgraph was recorded with 2 keV X-rays. The densitometer trace was taken along XX, 1.9 ns after peak of laser pulse.

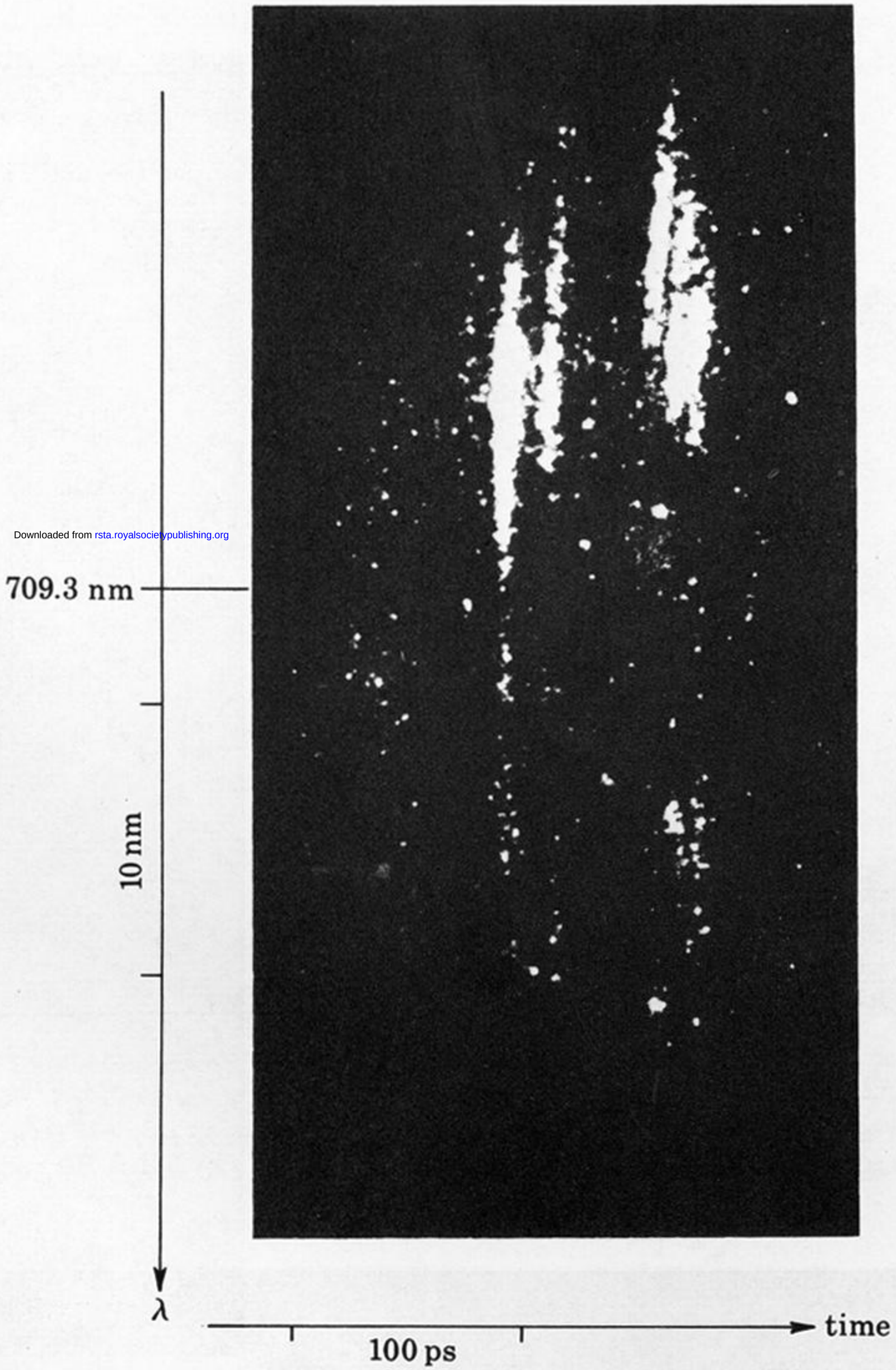

GURE 10. Streaked spectrum of $\frac{3}{2}\omega_L$ emission from a microballoon target irradiated at *ca.* 10^{16} W cm^{-2} with a 100 ps 1.06 μm pulse.

PHILOSOPHICAL TRANSACTIONS OF THE ROYAL SOCIETY A MATHEMATICAL, PHYSICAL & ENGINEERING SCIENCES

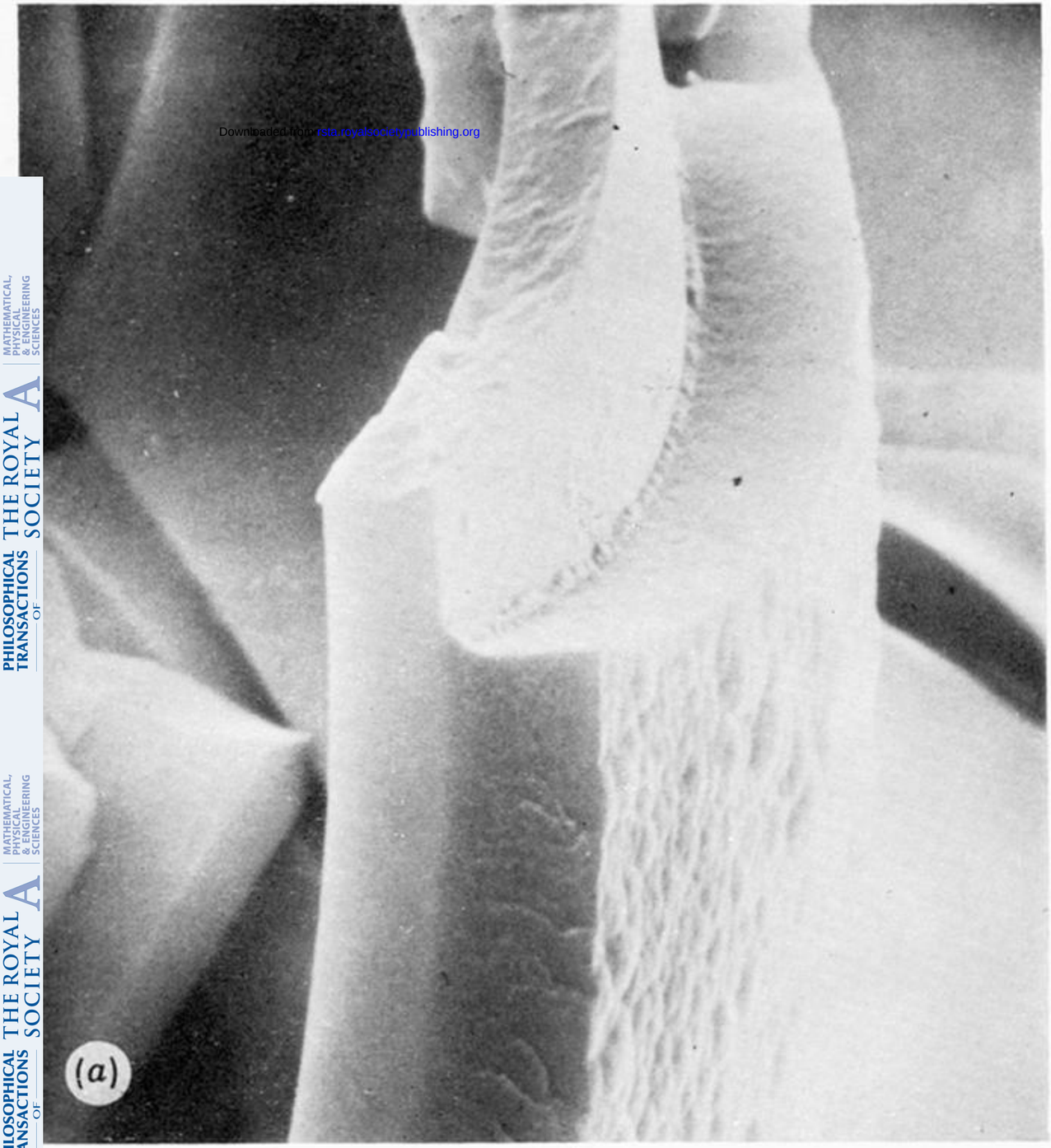

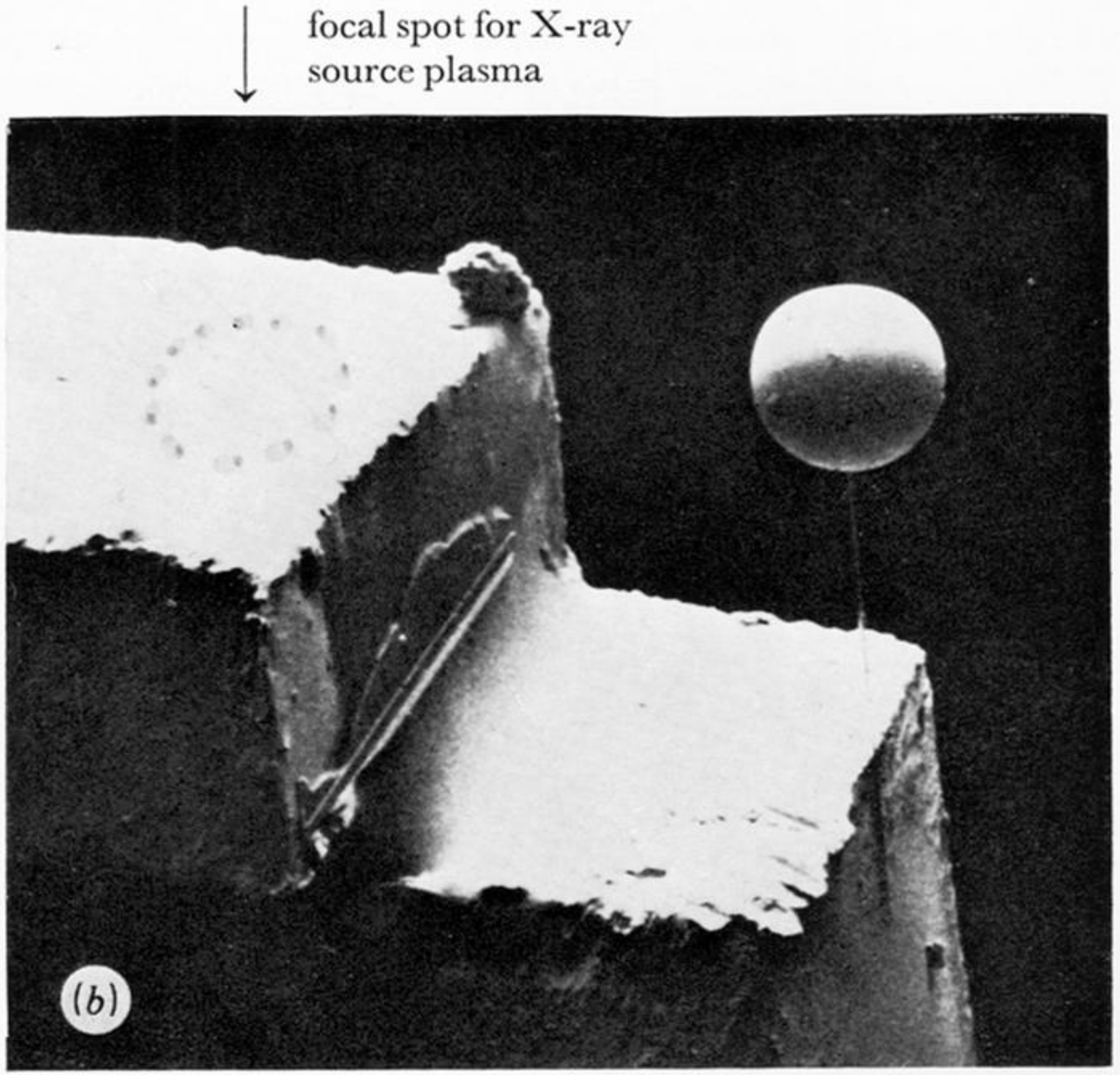

FIGURE 9. (*a*) Electron micrograph of a section of a polymer-coated target with a 2 μm polymer layer. (*b*) Electron micrograph of a polymer-coated glass microballoon mounted for X-ray streak shadowgraphy as a figure 6.